Formability optimisation of fabric preforms by controlling material draw-in through in-plane constraints

S Chen, L T Harper*, A Endruweit, N A Warrior
Polymer Composites Group, Division of Materials, Mechanics and Structures,
Faculty of Engineering, University of Nottingham, UK, NG7 2RD
* lee.harper@nottingham.ac.uk , Tel +44 (0)115 9513823

Abstract

A genetic algorithm is coupled with a finite element model to optimise the arrangement of constraints for a composite press-forming study. A series of springs are used to locally apply in-plane tension through clamps to the fibre preform to control material draw-in. The optimisation procedure seeks to minimise local in-plane shear angles by determining the optimum location and size of constraining clamps, and the stiffness of connected springs. Results are presented for a double-dome geometry, which are validated against data from the literature. Controlling material draw-in using in-plane constraints around the blank perimeter is an effective way of homogenising the global shear angle distribution and minimising the maximum value. The peak shear angle in the double-dome example was successfully reduced from 48.2° to 37.2° following a two-stage optimisation process.

Keywords

A. Fabrics/textiles; C. Finite Element Analysis; E. Forming

1 Introduction

In the manufacture of composite components, draping of reinforcement fabrics can cause large local shear deformations (change in fibre orientations, fibre volume fraction, fabric thickness, etc.) to occur. For most fabrics, in-plane shear is the main deformation mechanism in drape, but excessive local shear can lead to wrinkling (i.e. out-of-plane buckling due to local compressive stresses) and fibre fracture [1]. To successfully drape a reinforcement without encountering unwanted wrinkles and defects, the main challenge is identifying optimum forming conditions. Among the processing parameters affecting fabric press forming, the distribution of the blank holder force (BHF) and the blank shape are two essential properties that should be optimised to improve the quality of the formed shape [2, 3]. To optimise these parameters, efforts have been made to develop simulation tools to facilitate parametric studies.

Kinematic drape simulation codes [4, 5] use a purely geometrical approach to compute fabric drape patterns, but whilst this method is computationally relatively inexpensive, there is no accounting for mechanical material properties or process conditions. Conversely, Finite Element (FE) simulations enable the physics of the forming problem to be modelled and are becoming a viable choice as computing resources improve. This approach enables the influence of process parameters, including contacts and friction between components to be studied, but more importantly can be used to indicate the likelihood of defects occurring during forming. To date, most FE forming studies have focused on capturing the deformation of fabrics accurately though implementation of suitable constitutive material models [6, 7], rather than focusing on optimising the forming process.

Procedures for optimisation of the forming process can be classified as direct or indirect. Indirect methods refer to trial and error approaches, which require experience to interpret the results and can be time consuming. Nonetheless, they are likely to be used for optimising composite forming processes, since the complex relationship between wrinkling strain and clamping force does not need to be formulated. Indirect methods have previously been used to optimise fabric blank size [2] and BHF distribution [3], in order to minimise wrinkle formation. The probability for wrinkles to occur was shown to increase as the blank size is reduced relative to the size of the punch, since the tension in the blank is released during the latter stage of the forming process [2]. A uniform BHF distribution produced the least wrinkles in forming a hemisphere. However, it was concluded that a segmented blank holder is required to further reduce the level of wrinkling, to vary the local pressure distribution as a function of intra-ply shear and compressive forces [3].

Direct optimisation methods rely on mathematical relationships between the processing parameters (BHF, blank shape, fabric pre-shear) and the objective function (describing shear angle, wrinkling etc.) to be formulated, and have been used extensively for optimising metal forming problems. They commonly employ Genetic Algorithms (GA) [8-11], which mimic natural selection processes to enable the strongest permutation of design variables to evolve, and inferior ones to fade out. GAs are not widely used for optimising composite forming problems, because they are computationally expensive. A GA was coupled with a kinematic drape model by Skordos et al. [5], where the drape start point, drape direction and the pre-shear angle of the fabric were defined as design parameters. Employing the GA reduced the CPU time to 30 % of that required for an exhaustive search [5]. Alternatively, a simplified FE model was used in conjunction with

a GA to optimise the BHF around the perimeter of the blank, with the objective of minimising wrinkling [12]. Results indicated that optimising the BHF successfully eliminated concentrated buckling of tows around the base of the hemisphere, without affecting the in-plane shear angle distribution.

This paper presents a GA coupled with a non-linear explicit FE model to optimise the draw-in of the blank during composite press-forming. Spring-loaded clamps are used to directly provide in-plane tension to the fabric, rather than applying a normal pressure (resulting in in-plane friction) through a blank holder. This technique has been discussed in the literature for thermoplastic forming [13, 14] and is currently used in the automotive industry in preforming of non-crimp fabric. It enables the blank to be heated easily if the fabric is bindered or pre-impregnated, as the clamps are situated outside of the heated region of the press. This arrangement also offers more flexibility in terms of controlling material draw-in, as the spring-loading for each clamp can be controlled independently, but results in increased complexity. The optimisation procedure seeks to determine the optimum location and size of each clamp and the stiffness of each spring controlling the local draw-in. The objective is to minimise the global in-plane shear angle of the fabric.

2 Modelling of fabric preforming using in-plane constraints

2.1 Fabric material model

A non-orthogonal constitutive model is employed in this work to describe the fabric behaviour during preforming, which was previously derived by the authors [15]. This macro-scale model was shown to effectively capture the dominant factors in fabric forming, including in-plane shear, fibre elongation and inter-tow/intra-ply slipping. This kind of non-orthogonal model is considered to be more accurate than an orthogonal model,

because it appropriately describes the anisotropic behaviour of biaxial materials under large shear deformation [17, 18]. A VFABRIC subroutine was developed in Abaqus/Explicit to implement the mechanical constitutive relations for woven fabrics. Comparisons against experimental data [15] indicated high levels of accuracy for the simulation results, which was not significantly compromised by time-scaling or mass-scaling employed to reduce CPU time.

2.2 Validation for forming model using in-plane constraints

Numerical tests have been performed to validate the material model against experimental data for the case where in-plane constraints are used to provide tension in the fabric to control draw-in [13, 18], rather than out-of-plane blank-holders. Material parameters were consistent with the values in the literature [19-22] for a balanced plain weave glass fibre/polypropylene commingled fabric. The value of Young's modulus was taken to be 35.4 GPa in each fibre direction and the shear modulus was described by a polynomial:

$$G_{12} = (6.7135|\gamma_{12}|^4 - 9.8228|\gamma_{12}|^3 + 6.3822|\gamma_{12}|^2 - 1.5928|\gamma_{12}| + 0.1948)\ \text{MPa} \qquad (1)$$

where γ_{12} is the in-plane shear angle in radians.

Validation was conducted using the same geometry and material properties as in the literature [13, 18]. The blank was a single 0°/90° ply at a thickness of 0.4 mm. The optimised blank shape described by Harrison et al. [13] was employed, and the ply was modelled using quadrilateral membrane elements (M3D4R). Tooling was considered to be rigid; Coulomb friction was adopted for both tooling-material and material-material contacts, with a coefficient of 0.2; displacement boundary conditions were applied to the punch, whilst in-plane spring elements were used to connect the edge of the blank to a rigid frame, in order to control blank slippage. The stiffness of the elastic 1D spring

elements was 0.20 N/mm on the short edges and 0.27 N/mm on the long edges of the rectangular frame [13].

A comparison of the shear angle distributions is presented in Fig. 1. Qualitatively, the outline shape of the final formed part from the simulation is in very close agreement with experimental data [13]. A quantitative analysis was performed by comparing the local shear angle at 20 discrete locations (Table 1). Two experimental repeats were performed [13], and the measurements from each of the four quadrants were averaged for each repeat. Fig. 1 indicates that the predicted shear angles from the numerical solution fall within the range of the experimental values, with deviations of generally less than 2° according to Table 1.

3 Methodology of in-plane constraint optimisation

3.1 General strategy

The initial blank size for the double-dome forming study discussed here was 470 mm × 270 mm with a thickness of 0.4 mm, and the ply was discretised into 5076 square membrane elements (M3D4R). The initial fibre orientations in the blank were at 0°/90°. Springs are arranged around the perimeter of the preform to control material draw-in, providing in-plane constraints during draping. The optimum design of this system is dependent on the geometrical arrangement (number, position and size) of the springs and their mechanical properties (stiffness). The optimisation procedure is split into two stages as shown in Fig. 2: (a) Step I: Clamping arrangement optimisation, (b) Step II: Spring stiffness optimisation. The first step determines sensible clamping positions to improve formability, by reducing the maximum global shear angle in the model. Compromises have to be made however, as it is not practical to constrain every position. The second

step determines optimum spring stiffnesses for the derived spring arrangement, therefore the final solution may not be the global optimum, but near-optimal.

This multi-stage approach makes the procedure independent of specific geometrical parameters, thus providing the flexibility for application to a variety of test geometries. Simultaneous optimisation could potentially be more cost-effective computationally and produce a more efficient solution, but only if a suitable mathematical description could be derived. However, this would require a specific new formulation of the optimisation problem for each forming task and would not enable routine application of the method.

3.2 Step I: Clamping arrangement optimisation

Each node around the perimeter of the blank is initially constrained by an individual spring element with the same initial stiffness (see Fig. 2a). The other end of the spring is fixed to a fully constrained rigid frame. The force constraining movement of the blank is always oriented along the spring element axis, extending the spring as the material draws into the tool while forming. The status of each node (i.e. constrained or unconstrained) is determined by the optimisation algorithm. When it is unconstrained, the spring element is removed.

The clamping arrangement optimisation is implemented using Matlab, as shown in Fig. 3. For each loop or "generation" in the GA, a group of constraint patterns called "individuals" is generated and Abaqus/Explicit input files are produced. The shear angle distribution in the deformed blank for each individual is determined from Abaqus/Explicit analyses and then returned to Matlab. The corresponding fitness value is determined from this data to check for convergence. This loop repeats until the optimum is achieved.

A binary encoding method is applied to formulate each individual in-plane constraining pattern for the optimisation algorithm. Each pattern represents a binomial-status series, which can be described numerically by the encoding scheme in Fig. 3. Each bit in the binary code represents one potential constraint position and its value corresponds to an "unconstrained" or "constrained" status (0 or 1). By using this encoding scheme, the physical problem can be converted into a mathematical problem to perform a series of GA manipulations to heuristically search for the optimum constraining pattern.

This geometry optimisation problem can be written as:

minimise $f\{c_1, c_2, \ldots, c_n; \gamma_{12}(x, y, z)\}$

$$\text{subject to } c_i = \begin{cases} 1, & \text{constrained} \\ 0, & \text{unconstrained} \end{cases} \quad (i = 1, 2, \ldots, n) \tag{2}$$

$$\gamma_{12}(x, y, z) \in [0°, 90°]$$

$$(x, y, z) \in \Omega_M$$

where $f\{.\}$ is the GA fitness function to describe the selection criterion of the constraining pattern, which is employed to assess the distribution of shear angles in the material field. The variable c_i is the ith optimisation variable, which denotes the constrained status at the ith potential position. n is the total number of potential positions, i.e. the number of nodes on the blank perimeter.

The fitness function is used to assess how well each individual constraining pattern has adapted to the assessment criteria. Its value reflects the relative distance from the optimum solution, where a smaller value is preferred. A maximum value criterion (MAXVC) has been adopted here due to faster convergence compared with the Weibull distribution quantile criterion (WBLQC) previously used [15], whilst maintaining acceptable accuracy. The objective is therefore to keep all local shear angles below the

locking angle, by minimising the maximum shear angle. The maximum can be derived from the finite element approximation for $|\gamma_{12}(x,y,z)|$. Thus,

$$f_{MAXVC}\{c_1, c_2, \ldots, c_n; \gamma_{12}(x, y, z)\} = \max_{(x,y,z)\in\Omega_M}\{|\gamma_{12}(x, y, z)|\} \approx \max_{i=1,2,\ldots,N}\{\gamma_i\} \quad (3)$$

where $f_{MAXVC}\{.\}$ denotes the fitness function using MAXVC, which aims to minimise the maximum shear angle; Ω_M is the spatial material region; $\gamma_{12}(x,y,z)$ is the continuous shear angle distribution in the material region, Ω_M; N is the total number of integration points; $|.|$ is the absolute value of the variable; $\gamma_i = |\gamma_{12}(x,y,z)|$ is the absolute value of the shear angle at the ith material point, (x_i,y_i,z_i). Since the constraining pattern influences the shear angle distribution, the value of f_{MAXVC} is used for quantitative assessment of the fitness.

The theoretical optimum positions from Step I cannot be directly used in Step II. It is impractical to constrain the end of each individual yarn around the perimeter of the blank in reality, thus neighbouring constraints need to be grouped together to form consolidated clamps. If the distance between two adjacent constrained positions is smaller than a threshold value, they are considered to be part of the same clamp. A minimum clamp size is also specified, and any isolated constraints are discarded. Additionally, clamps are removed or split if they generate excessive curvature around the perimeter of the blank or increase MAXVC. The stiffness of each constraint is directly obtained by summing the stiffnesses of all parallel springs associated with each individual clamp. These compromises are essential for successful industrial implementation, but their negative impact can be alleviated to some extent by optimising the spring properties in Step II. Here, these practical considerations have been implemented manually, which is facilitated by the two-stage optimisation approach. Whilst it would be feasible to include them in the optimisation code as additional constraints or regularisation terms, as previously discussed by Skordos et al. [12], this would increase the number of variables in the

objective function. This would largely reduce the efficiency in automatically creating FE models, and the number of geometry variables may change during the optimisation, significantly increasing complexity. A potential solution would be to define a large enough number of variables and reserve sufficient memory, but this would be wasteful, causing computational resources to become redundant.

Since all nodes along the edges were initially connected to springs in Step I, it was necessary to choose a relatively low starting stiffness from the available range to avoid over-constraining the blank. In this step, the constraint stiffness was set to 0.03 N/mm at each applied position.

3.3 Step II: Spring stiffness optimisation

In-plane constraints are applied at the selected clusters of nodes identified in Step I (see Fig. 2b). A subsequent optimisation step is performed using a GA to determine optimum stiffness values for each spring from a user-defined range.

For simplification, only linear behaviour is considered, which can be parameterised as

$$F_i^{ct} = k_i^{ct}\, d_i^{ct} \quad (i = 1, 2, \ldots, m) \tag{4}$$

where m is the number of constrained clamping positions after refinement, k_i^{ct} is the stiffness of the ith spring, d_i^{ct} is the in-plane displacement at the ith constrained position, and F_i^{ct} is the corresponding constraining force. Consequently, the optimisation variables are converted into a stiffness k_i^{ct} (i = 1, 2, … , m). This method is also suitable for modelling non-linear behaviour, as the optimisation method is intrinsically the same, but the number of parameters increases.

The optimisation problem in Step II can be described as

minimise $f\{k_1^{ct}, k_2^{ct}, \ldots, k_m^{ct}; \gamma_{12}(x, y, z)\}$

subject to $k_i^{ct} \in [(k_i^{ct})^{low}, (k_i^{ct})^{upp}] \quad (i = 1, 2, \ldots, m)$

where $[(k_i^{ct})^{low}, (k_i^{ct})^{upp}]$ is the applicable stiffness range of the *i*th constraint. Similarly, MAXVC is employed again as the fitness function to minimise the maximum shear angle in Step II

$$f_{MAXVC}\{k_1^{ct}, k_2^{ct}, \ldots, k_m^{ct}; \gamma_{12}(x, y, z)\} = \max_{(x,y,z)\in\Omega_M} \{|\gamma_{12}(x, y, z)|\} \approx \max_{i=1,2,\ldots,N} \{\gamma_i\} \quad (5)$$

In this step, optimisation is aimed at finding a near-optimal solution to reduce the negative influence induced by manually refining the constrained positions. A summary of the GA is presented in Fig. 4.

3.4 GA stability analysis

The stability of a GA in delivering an optimum solution depends on the diversity of the population. This is determined by the population size, the initial population and probabilities for crossover and mutation. The population size has been chosen to be greater than the number of optimisation variables, for example using 100 for Step I (76 variables corresponding to 76 clamping positions per quarter model). The initial population is determined randomly to ensure sufficient diversity. The crossover probability (i.e. the proportion of each population where genes from individuals in the previous generation are recombined) was 0.8, a compromise between evolution rate and solution accuracy. The mutation probability enables a small random variation in the individuals of each generation to create new genes, ensuring genetic diversity and enhancing the probability for an improved fitness score. Its value was determined adaptively for this study, based on the fitness scores from the previous generation.

It is important to ensure that the initial population is distributed across the entire solution space to avoid restricting the range for the optimum value. The distance between

individuals in the solution space is therefore measured to quantify the diversity of the population. For the example of the 76 variables in Step I, the average distance between individuals must be less than the maximum value of 8.7 (i.e. $76^{1/2}$ for 76 binary variables). Furthermore, the average distance should progressively decrease for subsequent generations, indicating a reduction in search space and convergence towards the global optimum.

4 Results and discussion

4.1 Clamping arrangement optimisation from Step I

Several generations of clamping patterns have been selected to illustrate the optimisation evolution for Step I (Fig. 5), indicating the reduction in number of constraints and the evolution rate. Each generation represents a summary of 100 individual constraining patterns, where the bars represent constrained locations. The initial population of 100 patterns for the zeroth generation was generated randomly, which then evolved into subsequent generations according to the GA. In the figure, all bars are initially a shade of red, which indicates that all of the constraint positions are represented similarly across the 100 patterns. The shade of red changes as the constraining pattern evolves for each subsequent generation, where a darker red (tending towards black) represents a higher frequency for that constrained position. A lighter shade of red represents a lower frequency, where white indicates complete removal of the constraint. As the fitness function converges, all remaining bars appear black, which indicates that all 100 patterns for that generation are in agreement.

Fig. 5 shows that some of the final constraint positions start to emerge as quickly as generation 7, with some bars already shown as black. By generation 14, some of the

weaker bars are removed and a symmetrical clamping pattern starts to develop. By generation 35, there are very few red bars remaining, with the status of only 20 % of the clamping positions uncertain at this stage. The final clamping pattern is determined after generation 43, which is confirmed by comparing with the outcome from generation 51.

The diversity of the population for each generation in Step I has been checked by evaluating the average distance between individuals, shown in Fig. 6a. For the first six generations the value is approximately 6, indicating that the initial population covers approximately 70 % (6/8.7) of the solution space. The average distance reduces by 1.6 % ($0.14/76^{1/2}$) for each subsequent generation, indicating that evolution is progressive, allowing sufficient opportunity for elite genes, (i.e. genes related to low fitness scores in terms of maximum shear angles), to survive during offspring creation.

Fig. 6b shows the evolution of the fitness scores for Step I. The magnitude of the adaptive Fitness Range is similar for each generation until the Best Fitness converges, implying that a wide search range has been adopted throughout. The range of the fitness score varies due to adaptive mutation. The optimum solution (i.e. convergence of the Best Fitness) is achieved during generation 31. Perturbations induced by further mutations during the next 12 generations (indicated by a non-zero fitness range) appear to have no influence on the optimal solution. Furthermore, the mutation probability reduces to zero following generation 43, after the optimal solution has been determined. Therefore, Fig. 6 confirms that the present diversity prevents local optimum solutions, random selection and instability.

The maximum shear angle decreases by 11.2°, from 48.2° for the fully constrained system (Fig. 7a) to 37.1° after all unconstrained springs have been removed (Fig 7b). However, practical implementation of the optimum pattern in Fig 7b is not feasible, since too many

individual springs are required to obtain the blank boundary conditions. Therefore, it is necessary to compromise and combine neighbouring clamps and eliminate isolated ones (see Fig. 7c). The minimum threshold distance between clamps was chosen to be 25 mm (equivalent to the width of 5 finite elements), and the minimum clamp length was also assumed to be 25 mm. In addition, the spring located at the mid-point of the short edge (see Fig. 7b) was removed, as this could not be combined into a single clamp due to the region of high curvature generated by the springs either side. Consequently, only two clamps were required along each of the short edges to maintain the optimum draw-in. The individual constrained positions from Fig. 7b were combined and reduced to 14 clamps, as shown in Fig 7c. The stiffness of each consolidated spring was directly obtained by summing the stiffness of all of the parallel springs belonging to each corresponding block. Table 2 provides a summary of the spring stiffnesses after Step I of the optimisation, including the length and position of the corresponding clamps.

Although the maximum shear angle increased by 3.4° in Fig. 7c compared with the result in Fig. 7b, this still yields an overall reduction in peak shear angle of 7.7° compared with the unoptimised case. In addition, the shear angle distribution in Fig. 7b indicates that wrinkling occurs along the long edges when constrained by individual springs, as there are local transitions in shear angle. However, these disappear in Fig. 7c when longer clamps are introduced along the edges. Constraining the blank using consolidated clamps homogenises the boundary constraints to eliminate undesirable wrinkling around the perimeter.

4.2 Stiffness optimisation from Step II

The spring stiffnesses from the solution in Step I (Fig. 7c) form the starting point of Step II. Half of the individuals for the zeroth generation used the same combination of constraint properties as the solution from Step I and the rest were generated randomly, which then evolved into subsequent generations according to the GA. The population size for the GA was 20 in each generation, and the tolerance for the fitness function was 0.05°. For the current work, the range of spring stiffnesses in this step was chosen to be from 0.03 N/mm to 0.50 N/mm. The stability of the optimisation for Step II was validated using the same methodology outlined for Step I. The fitness scores confirmed that the initial population was suitably diverse, and Fig. 8a indicates that the solution was stable.

As shown in Fig. 8a, the maximum shear angle is reduced to 37.2° by optimising the spring stiffnesses. This value differs by 0.1° from the ideal optimum (37.1°) in Step I (see in Fig. 7b). It indicates that the negative influence induced by artificially adjusting the constrained positions is minimised by seeking an optimal combination of clamp stiffnesses in Step II, whilst making the solution more practical. Comparison of the maximum shear angles during each step therefore confirms that the two-stage optimisation does not significantly compromise the optimisation outcome. Using a more generic GA approach may enable both optimisation stages to be combined (e.g. assigning different sets of genes defining positions and stiffnesses) to further improve the accuracy of the solution. However, this would require variable encoding lengths to be used for the different parameters. Encoding the task as a single step optimisation problem may result in a more efficient solution in the longer term, but it would be more complex to implement and would only be applicable to this specific geometry.

The convergence of the spring stiffnesses for Step II is presented in Fig. 8b. The optimum combination of spring stiffnesses is presented in Table 2 and illustrated schematically in Fig. 9. This figure allows a general strategy for spring placement to be derived: At zones of the component geometry with small curvature, springs with relatively low stiffness are attached through long clamps to provide near uni-axial tension. Zones with a high degree of curvature require multiple springs with stiffnesses adapted to suit the fibre orientation, which are attached through short localised clamps, allowing for multi-axial tension to be applied to the blank. In general, springs attached to the clamps along the long edges have a stiffness of 0.20 N/mm, and springs along the short edges are approximately 0.30 N/mm for the current geometry. These are of similar magnitude to those used by Harrison et al. [13], where fewer clamps were used, and the stiffer springs were placed on the long edges. Figure 10 illustrates in-plane strains along the two principal fibre directions, where only negative strains are shown. These negative strains indicate fabric compression, which may result in localised wrinkles. The progression of the images implies that maximum strains along both fibre orientations have been reduced through strain homogenisation during optimisation, resulting in a reduction of potential regions of severe wrinkling. Whilst the shear angle distribution was the optimisation objective, the distribution of wrinkling strain is simultaneously homogenised as previously seen in a recent study [15].

5 Conclusions

A scenario has been introduced for controlling material draw-in during reinforcement forming processes, using a series of in-plane springs to locally apply tension to the preform, rather than using a blank holder to compress the preform out-of-plane and apply constraints through friction. A non-orthogonal constitutive relation has been defined for

bi-axial materials with large deformation, based on a VFABRIC model in Abaqus/Explicit. The in-plane constraints around the edges were modelled using spring elements connected to a fully constrained rigid frame, providing axial forces to control material slippage into the cavity.

An optimisation methodology has been developed by combining the explicit FE model with a genetic algorithm to optimise parameters associated with the in-plane constraints. It has been implemented in two stages: (a) Step I: Clamping arrangement optimisation, (b) Step II: Spring stiffness Optimisation. Process optimisation has been demonstrated using a double-dome geometry from the literature. Results indicate that controlling material draw-in by constraining the blank in-plane around the perimeter is an effective way of homogenising the global shear angle distribution and minimising the local maximum value. The peak shear angle was reduced from 48.2° to 37.2° following the two-stage optimisation process. Strains along the two principal fibre directions have also been reduced during the optimisation, through strain homogenisation, resulting in a reduction of potential regions of severe wrinkling.

Acknowledgements

The work presented in this paper was completed as part of the “Affordable Lightweighting Through Pre-form Automation” (ALPA) project. The authors gratefully acknowledge the financial support of the Technology Strategy Board and technical support from the project partners: McLaren Automotive, Formax, the Advanced Manufacturing Research Centre and the Manufacturing Technology Centre.

References

[1] Long AC, Clifford MJ. Composite forming mechanisms and materials characterisation. In: Long AC, editor. *Composite forming technologies*. Cambridge: Woodhead Publishing Ltd., 2007. p. 1-21.

[2] Lin H, Wang J, Long AC, Clifford MJ, Harrison P. Predictive modelling for optimization of textile composite forming. *Compos Sci Technol* 2007; 67(15–16): 3242-3252.

[3] Yu WR, Harrison P, Long AC. Finite element forming simulation for non-crimp fabrics using a non-orthogonal constitutive equation. *Compos Part A-Appl S* 2005; 36(8): 1079-1093.

[4] Van Der Weeën F. Algorithms for draping fabrics on doubly-curved surfaces. *Int J Numer Meth Eng* 1991; 31(7): 1415-1426.

[5] Skordos AA, Sutcliffe MP, Klintworth JW, Adolfsson P. Multi-objective optimisation of woven composite draping using genetic algorithms. In: *27th International Conference SAMPE Europe*. Paris, 2006.

[6] Yu WR, Pourboghrat F, Chung K, Zampaloni M, Kang TJ. Non-orthogonal constitutive equation for woven fabric reinforced thermoplastic composites. *Compos Part A-Appl S* 2002; 33(8): 1095-1105.

[7] Xue P, Peng X, Cao J. A non-orthogonal constitutive model for characterizing woven composites. *Compos Part A-Appl S* 2003; 34(2): 183-193.

[8] Wei L, Yuying Y. Multi-objective optimization of sheet metal forming process using Pareto-based genetic algorithm. *J Mater Process Tech* 2008; 208(1–3): 499-506.

[9] Conceição António CA, Magalhães Dourado N. Metal-forming process optimisation by inverse evolutionary search. *J Mater Process Tech* 2002; 121(2–3): 403-413.

[10] Chung JS, Hwang SM. Application of a genetic algorithm to process optimal design in non-isothermal metal forming. *J Mater Process Tech* 1998; 80–81: 136-143.

[11] Kahhal P, Brooghani S, Azodi H. Multi-objective Optimization of Sheet Metal Forming Die Using Genetic Algorithm Coupled with RSM and FEA. *Journal of Failure Analysis and Prevention* 2013; 13(6): 771-778.

[12] Skordos AA, Aceves CM, Sutcliffe MPF. Drape optimisation in woven composite manufacturing. In: *5th International Conference on Inverse Problems in Engineering: Theory and Practice*. Cambridge, 2005.

[13] Harrison P, Gomes R, Curado-Correia N. Press forming a 0/90 cross-ply advanced thermoplastic composite using the double-dome benchmark geometry. *Compos Part A-Appl S* 2013; 54: 56-69.

[14] Willems A. Forming simulation of textile reinforced composite shell structures. PhD dissertation, Katholieke Universiteit Leuven, 2008.

[15] Chen S, Endruweit A, Harper LT, Warrior NA. Inter-ply stitching optimisation of highly drapeable multi-ply preforms. *Compos Part A-Appl S* 2015; 71: 144-156.

[16] Peng X, Cao J. A dual homogenization and finite element approach for material characterization of textile composites. *Compos Part B-Eng* 2002; 33(1): 45-56.

[17] Peng X, Cao J. A continuum mechanics-based non-orthogonal constitutive model for woven composite fabrics. *Compos Part A-Appl S* 2005; 36(6): 859-874.

[18] Harrison P, Gomes R, Correia N, Abdiwi F, Yu WR. Press forming the double-dome benchmark geometry using a 0/90 uniaxial cross-ply advanced thermoplastic composite. In: *15th European Conference on Composite Materials*. Venice, 2012.

[19] Khan MA. Numerical and Experimental Forming Analyses of Textile Composite Reiforcements Based on a Hypoelastic Behaviour. PhD dissertation, Institut National des Sciences Appliquees de Lyon, 2009.

[20] Khan MA, Mabrouki T, Vidal-Sallé E, Boisse P. Numerical and experimental analyses of woven composite reinforcement forming using a hypoelastic behaviour. Application to the double dome benchmark. *J Mater Process Tech* 2010; 210(2): 378-388.

[21] Cao J, Akkerman R, Boisse P, Chen J, Cheng HS, de Graaf EF, Gorczyca JL, Harrison P, Hivet G, Launay J, Lee W, Liu L, Lomov SV, Long A, de Luycker E, Morestin F, Padvoiskis J, Peng XQ, Sherwood J, Stoilova Tz, Tao XM, Verpoest I, Willems A, Wiggers J, Yu TX, Zhu B. Characterization of mechanical behavior of woven fabrics: experimental methods and benchmark results. *Compos Part A-Appl S* 2008; 39(6): 1037-1053.

[22] Peng X, Rehman ZU. Textile composite double dome stamping simulation using a non-orthogonal constitutive model. *Compos Sci Technol* 2011; 71(8): 1075-1081.

Tables

Table 1. Comparison of shear angle data from Abaqus/Explicit VFABRIC model against two sets of experimental results from literature [14].

ID	coord. (mm)		shear angle (deg.)			ID	coord. (mm)		shear angle (deg.)		
	x	*y*	exp. (case 1)	exp. (case 2)	num.		*x*	*y*	exp. (case 1)	exp. (case 2)	num.
1	85	65	4.4 ± 2.9	3.3 ± 0.8	2.0	11	17.3	202.7	7.6 ± 1.5	6.2 ± 1.9	7.8
2	60	40	0.1 ± 0.5	0.1 ± 0.4	0.3	12	26	188	14.1 ± 0.7	13.7 ± 1.1	14.3
3	45	40	0.3 ± 0.3	0.3 ± 0.5	0.4	13	34.7	171.8	14.5 ± 2.1	15.2 ± 0.7	15.6
4	10	40	-0.4 ± 1.1	0.5 ± 1.1	0.7	14	44.6	155.9	22.3 ± 2.4	23.3 ± 1.9	25.0
5	60	80	3.7 ± 1.4	3.0 ± 2.0	2.8	15	52	142.1	31.5 ± 2.3	32.1 ± 2.1	32.8
6	45	80	0.5 ± 1.3	-0.5 ± 1.6	1.4	16	60	127.6	29.2 ± 1.8	29.1 ± 1.3	31.0
7	10	80	1.4 ± 1.4	-0.9 ± 0.9	2.7	17	68.9	112.6	15.8 ± 1.5	12.7 ± 3.0	12.1
8	25	120	11.9 ± 1.2	14.0 ± 2.1	12.1	18	77.1	97.2	4.0 ± 0.6	2.1 ± 2.7	4.7
9	5	140	7.0 ± 1.1	6.9 ± 0.4	7.0	19	84.9	83.4	4.1 ± 1.1	1.3 ± 2.9	5.0
10	15	160	10.4 ± 0.6	11.8 ± 0.9	10.7	20	94.4	67.4	5.5 ± 2.5	1.0 ± 3.9	4.1

Table 2. Clamping parameters obtained from Step I and Step II (The origin of the undeformed coordinate system is the centre of the blank).

clamp	central edge position		clamp length	stiffness (N/mm)	
	undef. *x* (mm)	undef. *y* (mm)	(mm)	Step I	Step II
k_1^{ct}	-135.0	0	160	0.39	0.21
k_2^{ct}	-135.0	130.0	40	0.27	0.21
k_3^{ct}	-135.0	212.5	25	0.09	0.19
k_4^{ct}	-40.0	235.0	40	0.21	0.28
k_5^{ct}	40.0	235.0	40	0.21	0.28
k_6^{ct}	135.0	212.5	25	0.09	0.19
k_7^{ct}	135.0	130.0	40	0.27	0.21
k_8^{ct}	135.0	0	160	0.39	0.21
k_9^{ct}	135.0	-130.0	40	0.27	0.21
k_{10}^{ct}	135.0	-212.5	25	0.09	0.19
k_{11}^{ct}	40.0	-235.0	40	0.21	0.28
k_{12}^{ct}	-40.0	-235.0	40	0.21	0.28
k_{13}^{ct}	-135.0	-212.5	25	0.09	0.19
k_{14}^{ct}	-135.0	130.0	40	0.27	0.21

Figures

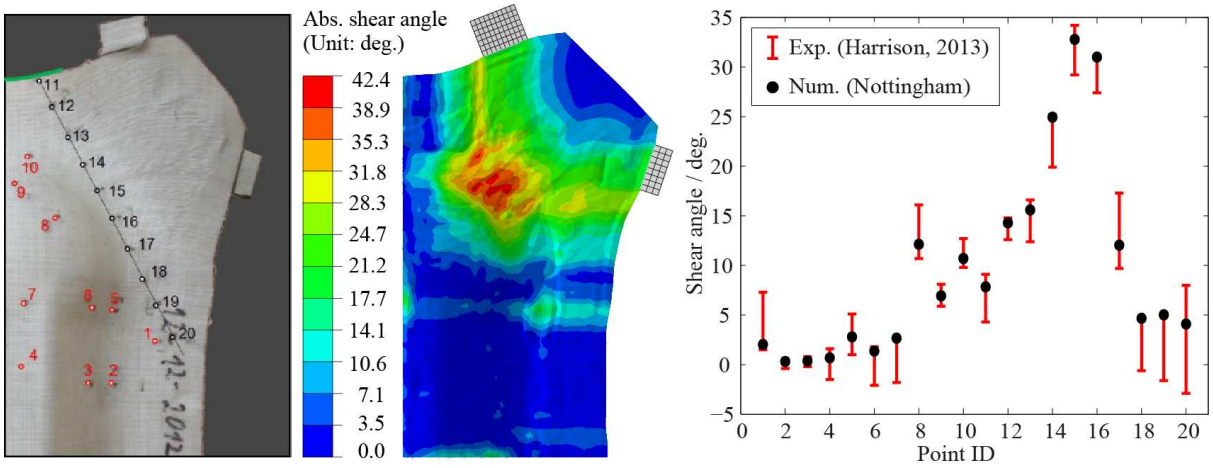

Fig. 1. Comparison of fabric forming model using in-plane constraints against experimental results from literature [14]; fibre orientation is 0°/90°.

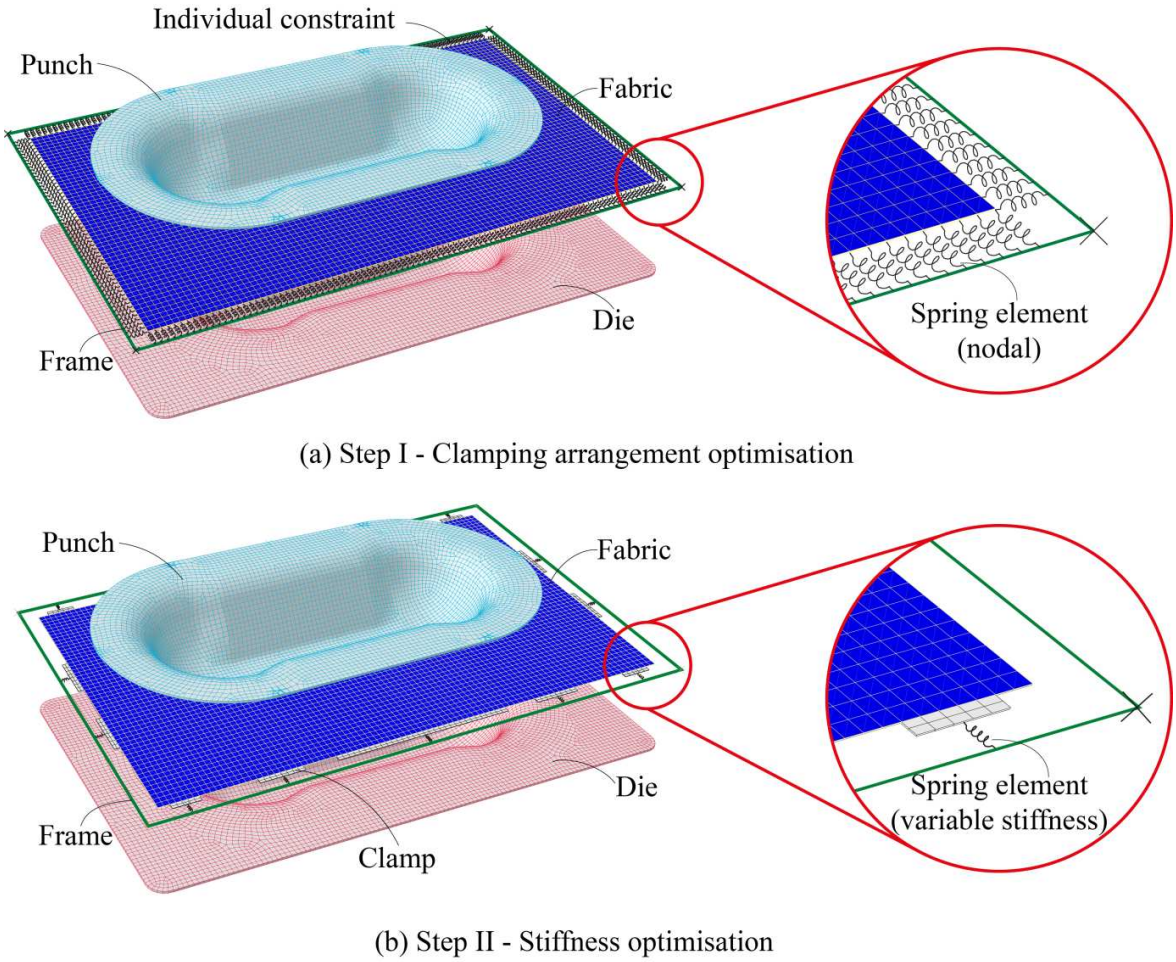

Fig. 2. Finite element models for two-step in-plane constraint optimisation.

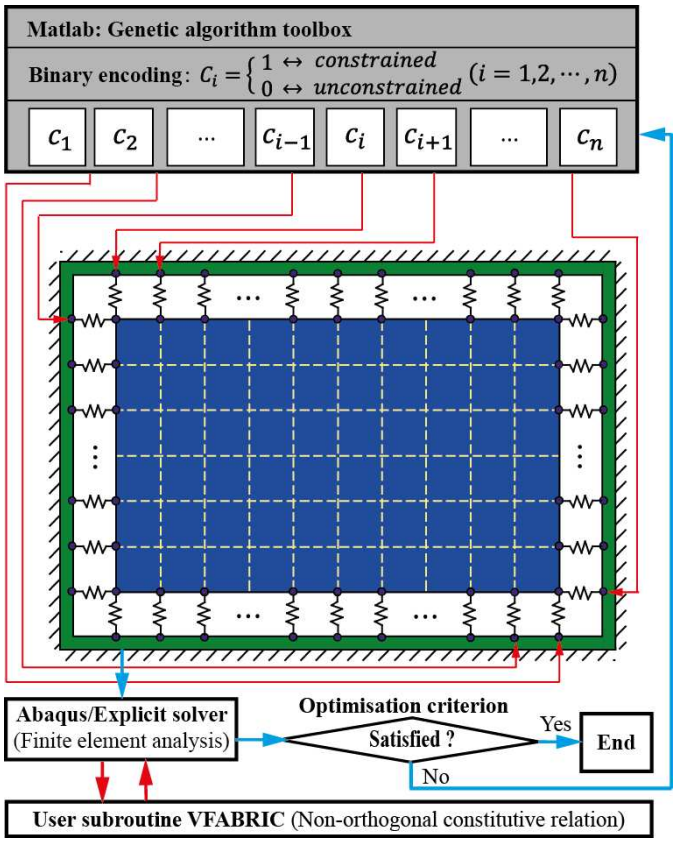

Fig. 3. Implementation of Step I - Geometry optimisation.

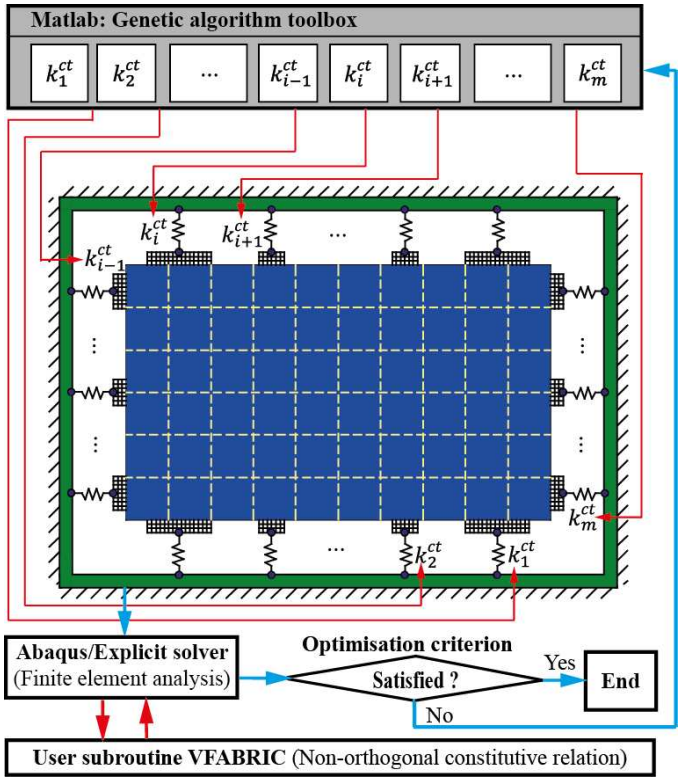

Fig. 4. Implementation of Step II - Near-optimisation of constraint properties.

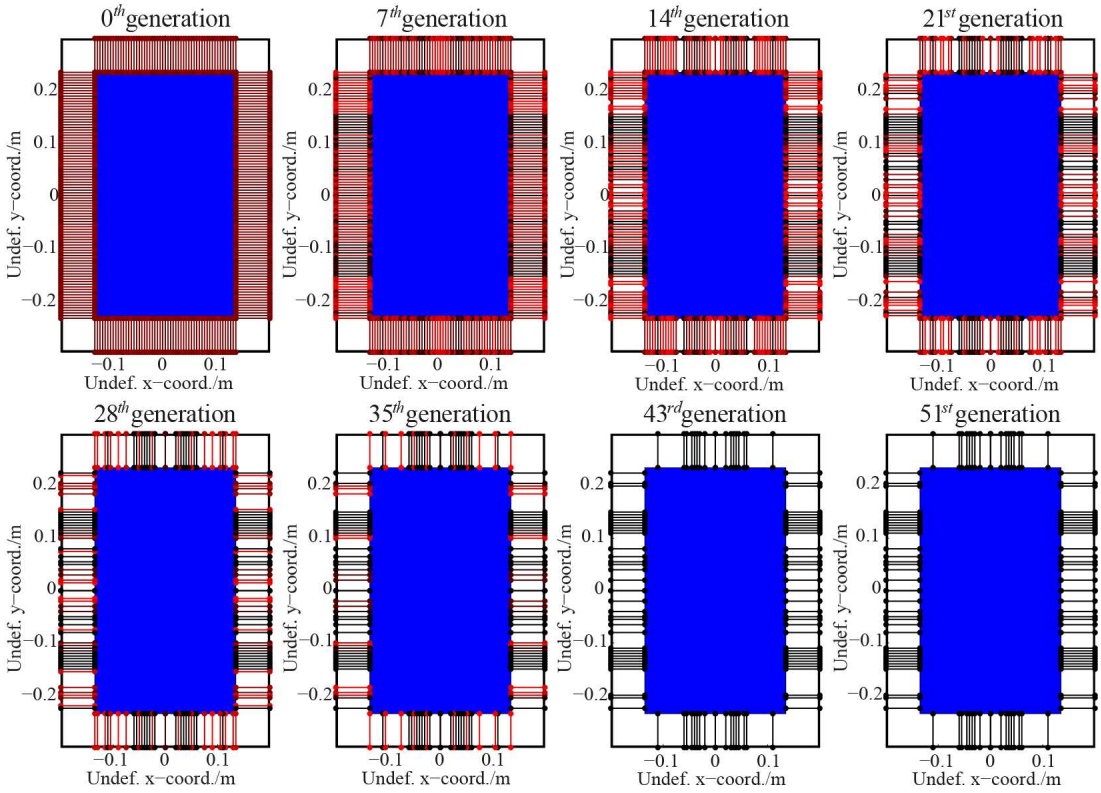

Fig. 5. Optimisation evolution of constraining pattern in Step I; solid bars represent constrained positions in the respective generation; red scale indicates the frequencies of occurrence within the respective generation.

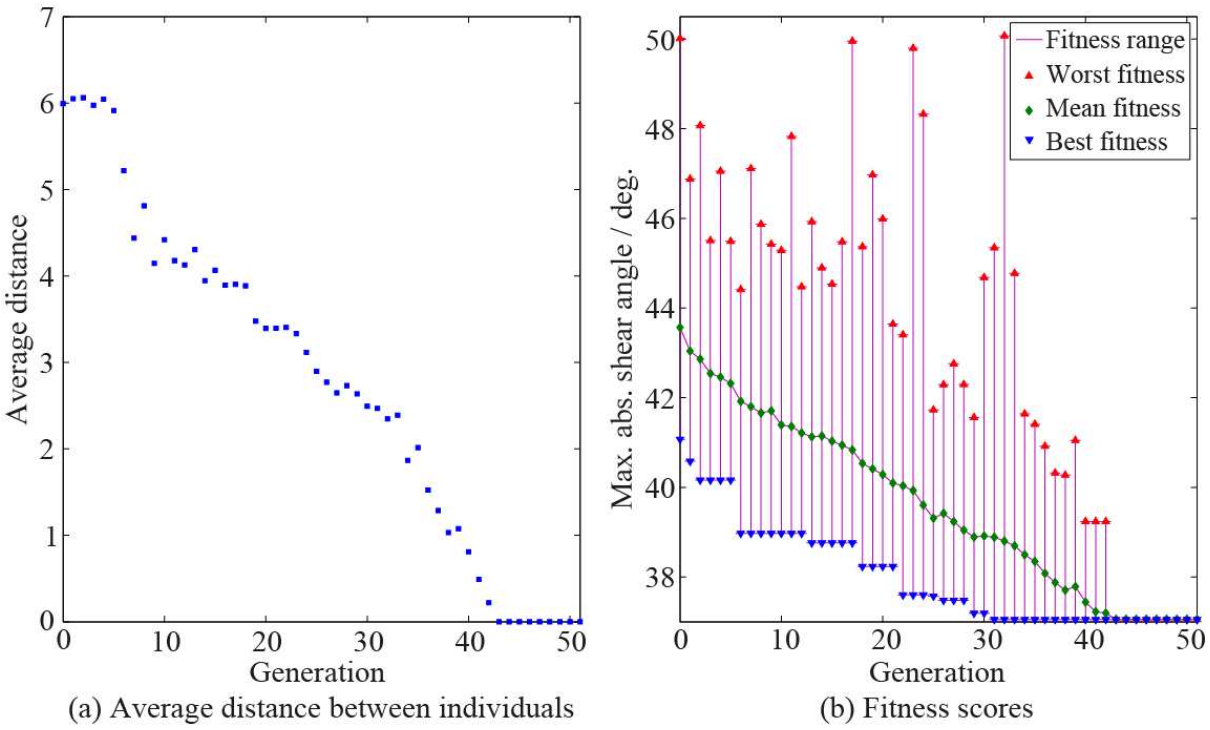

Fig. 6. (a) Population diversity and (b) optimisation evolution for Step I.

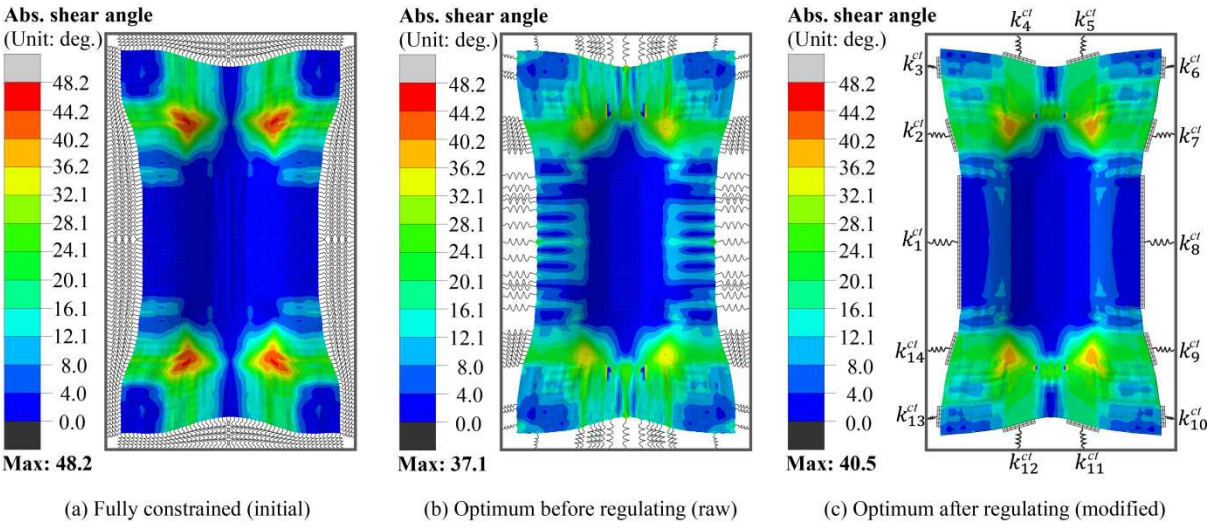

Fig. 7. Step I – Clamping arrangement optimisation for a single 0°/90° ply.

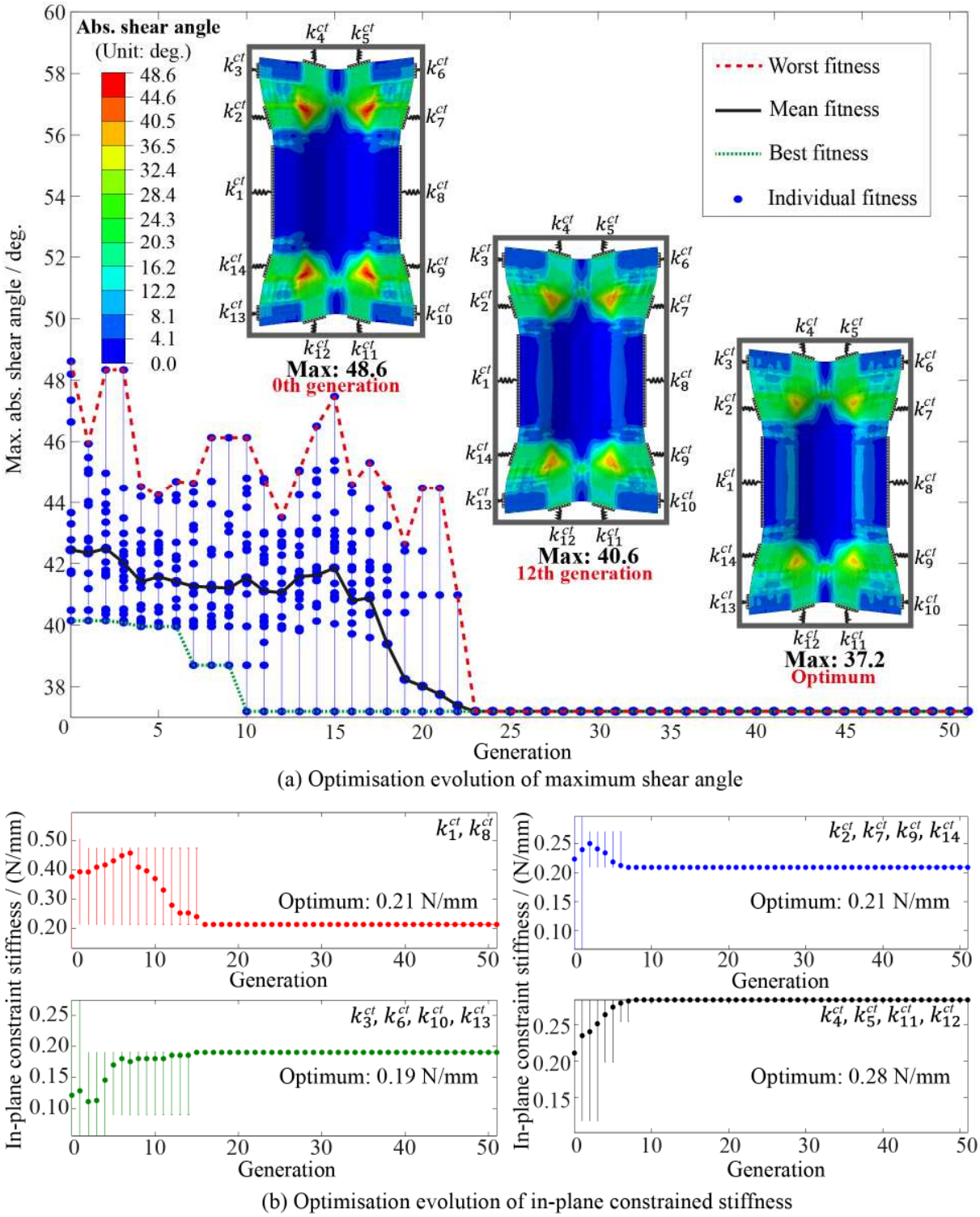

Fig. 8. Step II – stiffness optimisation for a single 0°/90° ply.

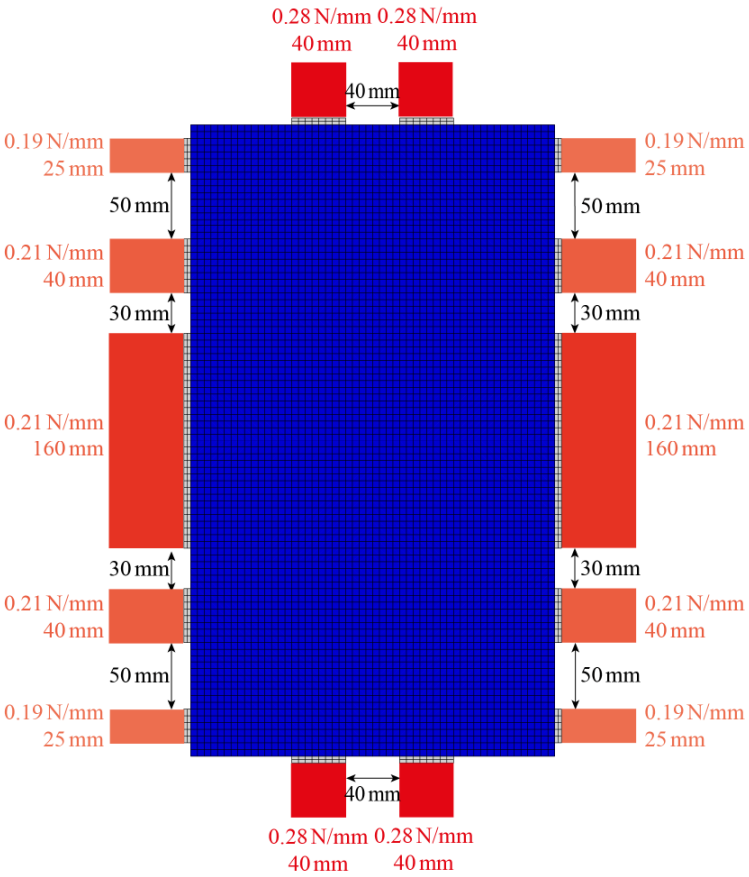

Fig. 9. Schematic of locations and widths of clamps; spring stiffnesses are also indicated.

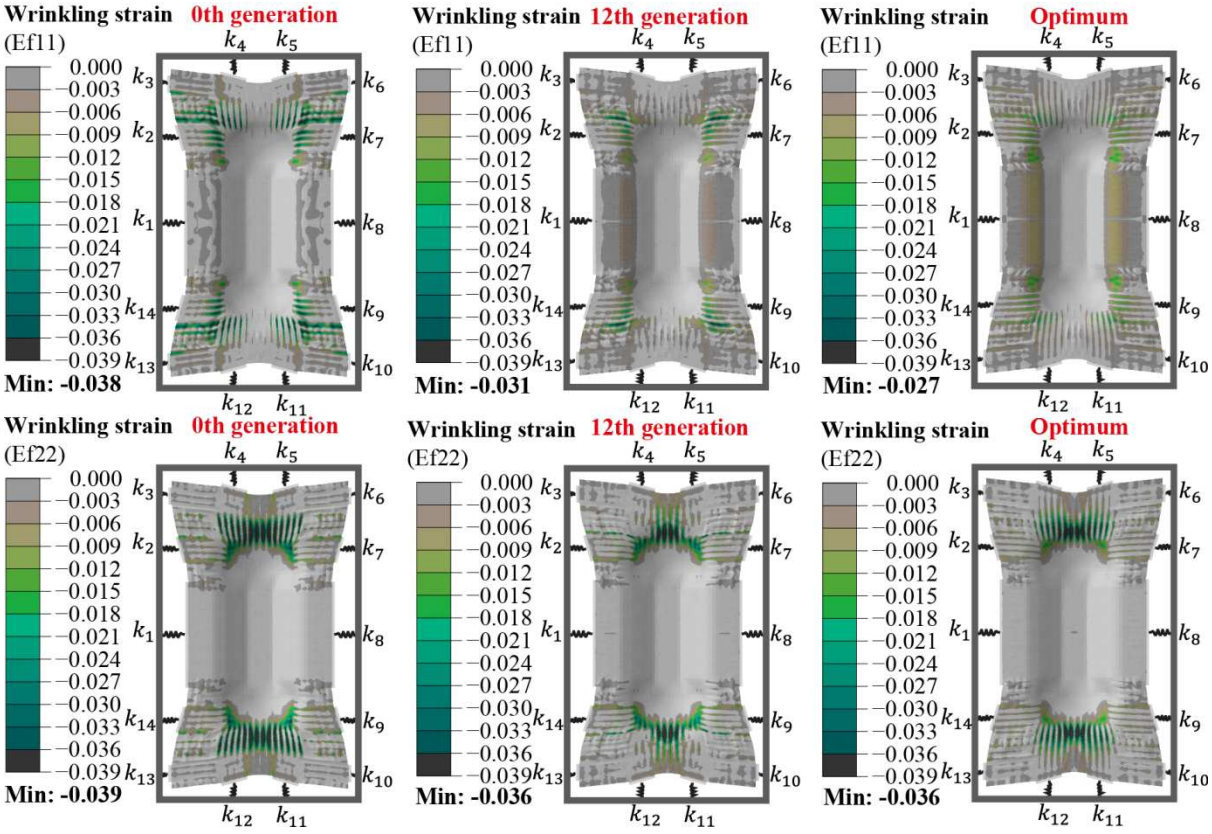

Fig. 10. Wrinkling strain along both principal fibre orientations.